XVII European Conference
ECSMGE 2019
Reykjavik
on Soil Mechanics
and Geotechnical Engineering

Monitoring and preliminary numerical interpretation of the interaction between an unstable rock cliff and the underlying soil deposit

Surveillance et interprétation numérique préliminaire de l'interaction entre une falaise rocheuse instable et le gisement de sol sous-jacent

L. Simeoni
Department of Civil, Environmental and Mechanical Engineering, University of Trento, Italy

F. Cecinato
Department of Earth Sciences "Ardito Desio", University of Milan, Italy

G. Dalla Porta
Department of Civil, Environmental and Mechanical Engineering, University of Trento, Italy

ABSTRACT: Complex landslide mechanisms involving both rock and soil material characterised by remarkably different stiffnesses are not straightforward to analyse numerically, especially if realistic displacement values are to be evaluated in their interaction with civil infrastructures. In this work, one of such landslides interacting with a viaduct occurring in Northern Italy is analysed. After a description of the landslide and the interpretation of relevant field measurements, the problem is analysed numerically by means of Finite Elements. A preliminary numerical interpretation of the gravitational phenomenon is provided, including the initial rock cliff degradation phase leading to the formation of a debris deposit and the subsequent development of rupture surfaces both in the rock and debris material. Comparison between simulations and field evidence suggests that the proposed numerical interpretation is realistic.

RÉSUMÉ: Les mécanismes complexes de glissement de terrain impliquant des matériaux de roche et de sol caractérisés par des rigidités remarquablement différentes ne sont pas faciles à analyser numériquement, en particulier si des valeurs de déplacement réalistes doivent être évaluées dans leur interaction avec les infrastructures civiles. Dans ce travail, un de ces glissements de terrain en interaction avec un viaduc dans le nord de l'Italie est analysé. Après une description du glissement de terrain et l'interprétation des mesures de terrain pertinentes, le problème est analysé numériquement à l'aide d'éléments finis. Une interprétation numérique préliminaire du phénomène gravitationnel est fournie, y compris la phase initiale de dégradation de la falaise rocheuse conduisant à la formation d'un dépôt de débris et au développement subséquent de surfaces de rupture dans le matériau rocheux et les débris. La comparaison entre simulations et données de terrain suggère que l'interprétation numérique proposée est réaliste.

Keywords: Landslide, Glacial valley, Numerical analysis, Stress distribution, Strain localisation

1 INTRODUCTION

The typical ‚U-shaped' morphology of glacial valleys may bring about the formation of very steep rocky sides, that are prone to instability phenomena such as rockfall, toppling and sliding. Whenever the mechanical rock properties are subject to progressive degradation (Lebourg et al., 2011), instability phenomena become more pronounced, causing debris accumulation at the cliff toe.

An example of the above described morphology is the alpine glacial valley of Isarco (North-eastern Italy), where landslide V70 is located. Landslide V70 was recognized to be a partial reactivation of a Deep-Seated Gravitational Slope Deformation (DSGSD) and it was classified as an active landslide (Simeoni et al., 2015) that has been causing the movement of the viaduct piers located at the toe of the slope (Figure 1).

Field measurements of the subsurface displacements were available only at the toe of the slope, near the viaduct piers, by which three different hypotheses for the sliding surface location were formulated (Figure 1). Sliding surface 1 would develop entirely within the debris deposit at the toe of the slope, while surfaces 2 and 3 would develop up to the first or second trench, respectively.

Recent measurements of the surface displacements revealed that movements of the rock cliff are greater than those occurring on the sliding surface identified below the piers.
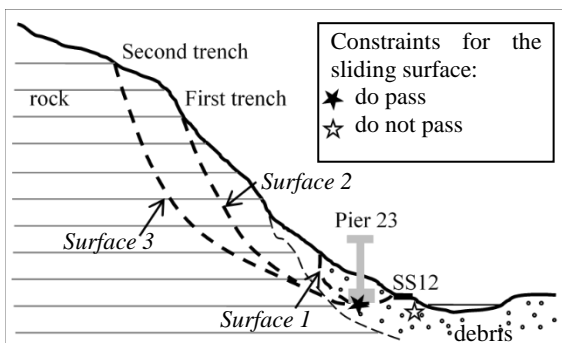
Assuming that the rock cliff is moving downwards, this paper describes some preliminary numerical Finite Element analyses carried out with Plaxis2D to investigate the interaction between the rock cliff and the underlying deposit of debris. With reference to a realistic post-glacial cross section, it was firstly investigated if a possible degradation of rock mechanical properties may have caused the failure of the rock slope. Then, the current slope geometry was analysed and the development of plastic points in the debris deposit due to the activation of sliding surfaces in the rock was investigated. Finally, the numerically obtained displacement field was compared to field measurements along one vertical.

2 FIELD MEASUREMENTS OF DISPLACEMENTS

Displacements of parts of the viaduct have been measured since 1993 by using different instrumentation such as theodolite and stadia rods, biaxial clinometers, direct pendula, Total Station, while inclinometers were used to measure the subsurface displacements in the periods 1993-2000 and from 2008 to present. Details of the above instrumentation may be
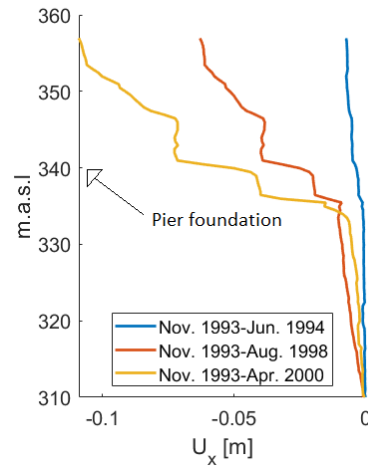

Figure 1. Example of cross section for landslide V70

Figure 2. Example of subsurface displacements close to Pier 23

found in Tombolato et al. (2011) and Simeoni et al. (2015).

Due to the small magnitude of displacements, significant efforts were spent to identify and to reduce systematic errors affecting the measurements. In particular, it was proved important to process total station measurements in terms of yearly rate of displacement, and to integrate inclinometer displacements locally, where the sliding surfaces were identified (Simeoni and Ferro, 2015).

Displacement rates on the sliding surface located below the piers resulted to be around 9 mm/year. Since 2012, further total station measurements have been carried out using targets installed on the rock cliffs, and displacement rates of more than 20 mm/year were estimated.

3 MECHANICAL PROPERTIES

The thickness of the debris was estimated from boreholes drilled at the toe of the slope to range from 15 to 20 m. The debris consists of weathered rock fragments and blocks of tuff and ignimbrite, accumulated at the foot of the cliffs (talus and rockfall deposit) and mixed with glacial sandy to clayey deposits and alluvial lenses at the base of the slope. The bedrock is made of Permian ignimbrite and a layer of 10-15 m of weathered and intensely crushed rock was detected between the bedrock and the debris. Permian ignimbrite and tuff outcrop at the rock cliff.

In addition, some piezometers were installed at the toe of the slope, indicating that the water table lies below the sliding surfaces.

3.1 Shear strength of debris

The shear strenght of the finer part of the debris was investigated by shear box tests on specimens that were reconstituted selecting the soil material with grain size $\leq$2 mm. The effective angles of shearing resistance at constant volume varied between 26° and 34°, while the angles of residual strength varied between 20° and 34° (i.e., in some

Table 1. Shear resistance and stiffness from GSI

GSI	c' (kPa)	φ' (°)	E (MPa)
25	152	27.2	1061
30	255	27.4	1414
35	407	27.5	1886
40	624	27.6	2515
45	934	27.7	3354
50	1377	27.7	4472

cases no frictional strength decay occurred during repeated shearing direction reversals). Peak strength parameters could be estimated from in situ dynamic penetration tests, resulting in a coesion c'_p=10 kPa and an angle of shearing resistance φ'_p=41°.

3.2 Shear strength of rock

An estimation of the rock shear strength was possible from the estimates of the outcrops' Geological Strength Index (GSI), and using the empirical relations suggested by Hoek et al. (2002). GSI=50 was thus assigned to the intact rock, and GSI=25 to the weathered rock. Accordingly, cohesion varied between 157 kPa and 1307 kPa and the angle of shearing resistance ranged from 27.2° to 27.7° (Table 1).

It is interesting to note that the estimated angles of shearing resistance depend only slightly on GSI, and are consistent with those obtained for the debris.

3.3 Soil and rock stiffnes

A Cross Hole test was carried out at the toe of the slope, down to a depth of 60 m. The obtained Young's modulus is plotted in Figure 3 against depth. An average value of about 900 MPa for a depth of 0-30 m represents the debris, the weathered rock is characterised by vaules of 2000-3000 MPa, while values of about 5000 MPa identify to the bedrock. The latter value is in accordance with that estimated for GSI=50 (see Table 1).
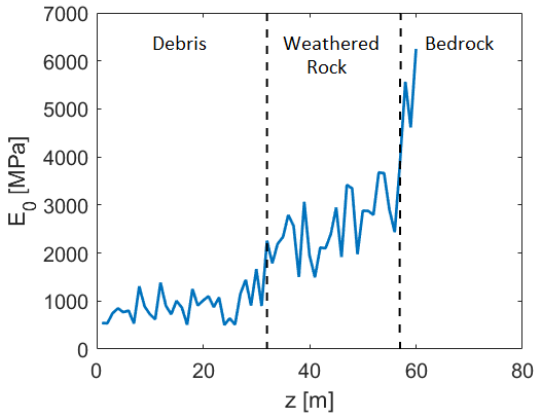
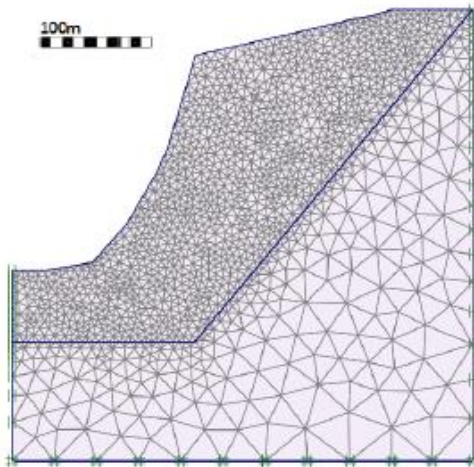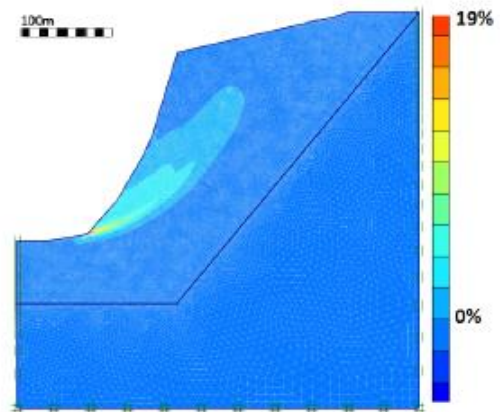Figure 3. Young's modulus obtained from the Cross Hole test

rock, starting from those corresponding to a GSI=50 (see Table 1), and adopting as Poisson's ratio ν=0.25. The Mohr-Coulomb constitutive law was assumed, with dilatancy angles ranging from 0° to ψ=φ'.

Results are shown in Figure 5. Localisation of shear strain occurs at GSI=40 for a non-associated flow rule (ψ=0°) and at GSI=35 for an associated flow rule (ψ=φ'=27.5°).

The outcome of the analysis suggests that it is plausible that the post-glacial slope failed due to the degradation of mechanical parameters. It is also likely, by looking at the results for ψ=0° (Figure 5), that more than one sliding surface developed.

Figure 4. Post-glacial geometry

4 STABILITY OF THE POST-GLACIAL SLOPE

The cross section shown in Figure 4 was assumed to represent the slope geometry after the melting of the glacier. It refers to an actual cross section of the cliff close to the V70 landslide location, but where debris has not been accumulated at the toe.

By using Plaxis2D, numerical Finite Element elasto-plastic analyses were carried out gradually decreasing the mechanical parameters of the

ψ=0°, GSI=40

ψ=φ'=27.5°, GSI=35

Figure 5. Shear deformation

After analysing the supposed post-glacial geometry, the next step was analysing the current slope geometry, with the debris at the toe and a reduced volume of rock at the top of the cliff. Two different materials were considered at this stage: rock and debris, exhibiting markedly different stiffnesses. In order to investigate the effect of stiffness contrast in the evaluation of initial stress conditions (so-called geostatic calculation step), preliminary analyses on a simple horizontal geometry model were carried out.

5 INITIAL CONDITIONS IN SOILS WITH DIFFERENT STIFFNESS

A horizontal deposit 5 m high and 60 m long was considered, longitudinally subdivided into two regions of soil with different stiffness: E_l on the left hand side and E_r on the rigth hand side. Considering E_r=1000 Mpa, stifness ratios $\eta=E_l/E_r$ ranging from 0.1 to 1 were investigated. Poisson's ratio ν=0.3 and unit weight γ=20 kN/m^3 were assumed for both soils.

An initial analysis involved running the geostatic calculation step assuming linear elastic behaviour (Figure 6 and Figure 7). Different cross-sections of the domain were considered, where ξ represents the distance of the considered section from the stiffness discontinuity, on the softer soil side, normalised with respect to domain height. It can be observed that horizontal stress increases while vertical stress decreases with decreasing stiffness ratio, while shear stress increases approaching the surface and the vertical discontinuity. As a consequence, shear stress levels close to the ground surface tend to violate the Mohr-Coulomb criterion.

Further, assuming for the softer soil c'=1 kPa and φ'=41°; for the stiffer soil c'=656 kPa and φ'=27°, the effect of interface elements located along the vertical discontinuity and of a further stiffness reduction at the top of the soft soil (iper-soft soil) was investigated with an elasto-plastic
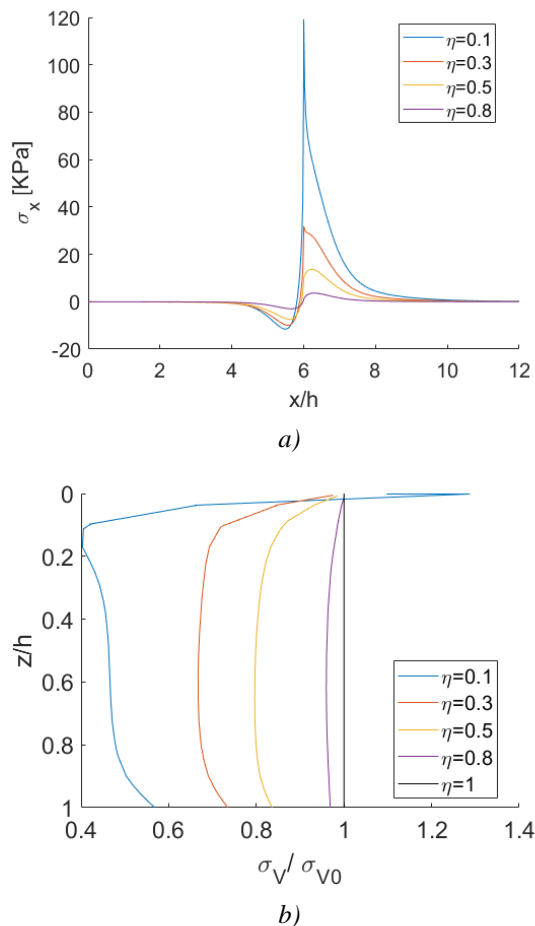

a)

b)

Figure 6. Stresses for different stiffness ratios $\eta=E_l/E_r$. a) horizontal stress along a cross section close to the ground surface; b) normalized vertical stress along the cross section at $\xi=0,10$.

analysis. Results are shown in Figure 8 for η=0.1 and a shear interface resistance with φ$_i$'=30°.

It can be observed that a more realistic initial condition could be obtained in the geostatic calculation step by introducing interface elements at the stiffness discontinuity and by reducing stiffness at the top of the softer soil.
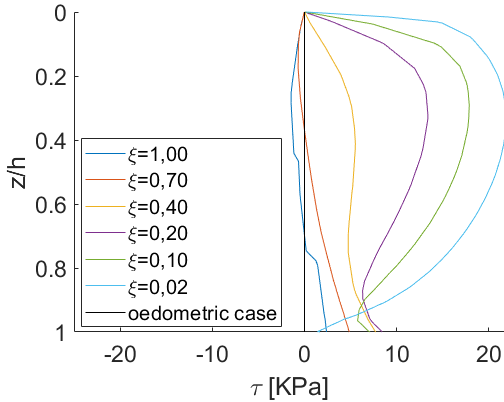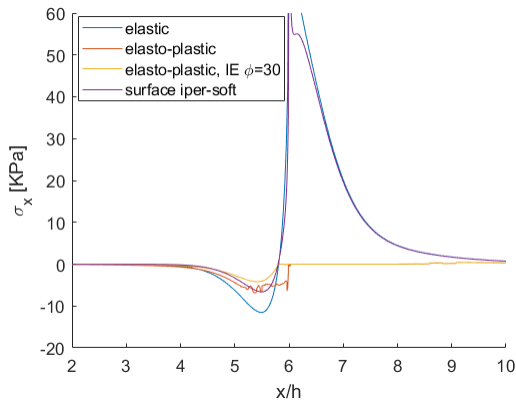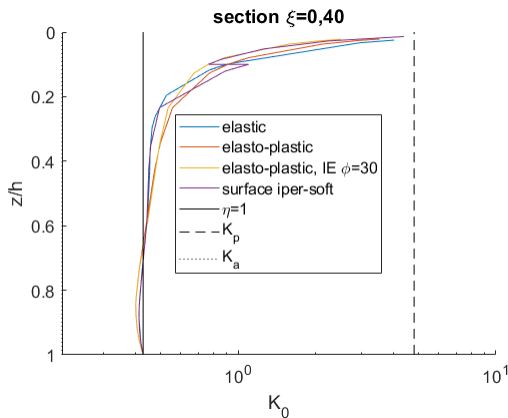
Figure 7. Shear stress for $\eta=o.1$ at different vertical cross sections.

a)

b)

Figure 8. a) horizontal stress sx and b) K0=sx/sz using Interface Elements and the iper-soft soil assumption.
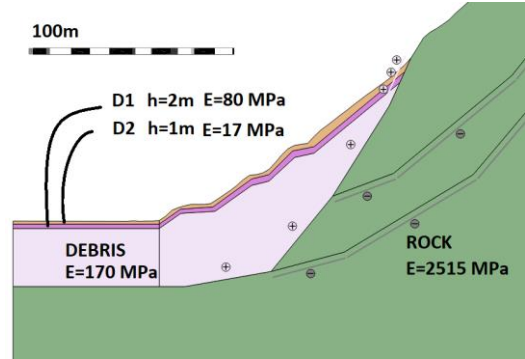

Figure 9. Current slope cross section. To achieve more realistic initial stress conditions, two soft layers at the top of debris and interface elements beteen debris and rock material were considered.

6 CLIFF ROCK-DEBRIS INTERACTION

The current slope geometry (whose cross-section is reported in Figure 9) was then analysed with an elasto-plastic numerical analysis.

Although the parametric study presented in Section 5 helped to identify the most suitable numerical settings to achieve the most realistic initial stress conditions (namely, considering two softer layers at the top of the debris and interface elements beteen debris and rock material), the development of a certain number of plastic points after the geostatic calculation step could not be avoided (Figure 10).

After the gravity loading step, an elasto-plastic analysis was performed, activating interface elements at the locations in the rock mass where the preliminary analysis of Section 4 had identified localised deformation.

Results in terms of displacement contours and location of plastic points are shown in Figure 11. It can be observed that the activation of sliding surfaces in the rock causes the concentration of plastic points in the debris mass (i) in the vicinity of the sliding surfaces and (ii) near the ground surface. Moreover, by plotting the simulated accumulated displacements (Figure 12), profiles are obtained that are compatible with the
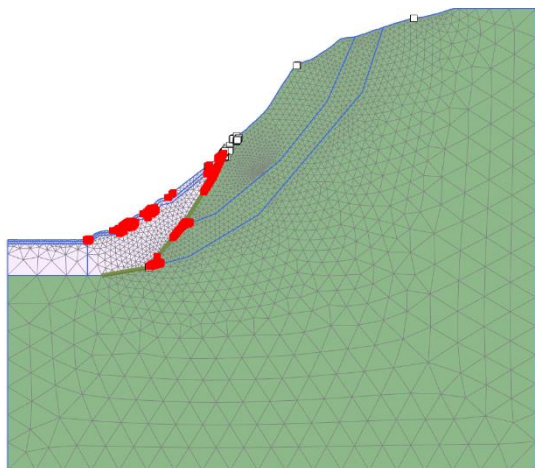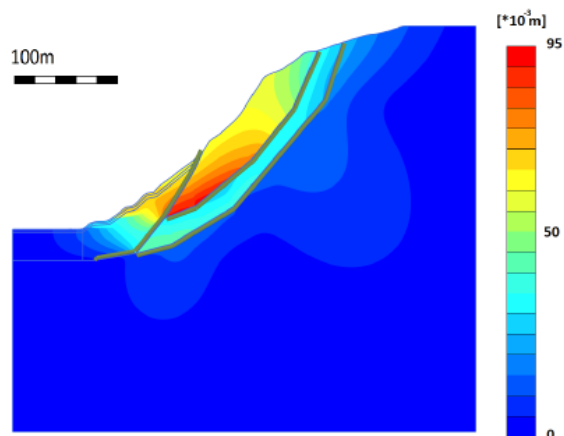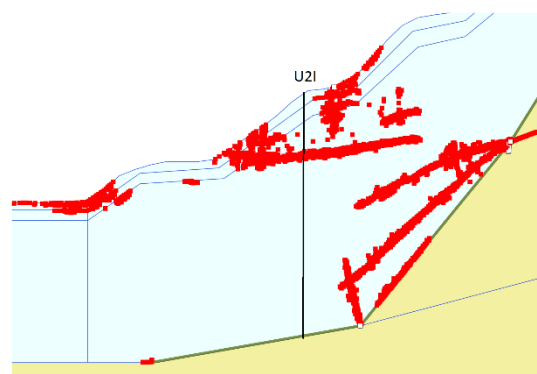
Figure 10. Plastic points obtained after the geostatic step.

mechanisms identified by field measurements. Compared to Figure 2, a slightly shallower sliding surface is simulated. However, it should be noted that the simulations currently do not account for the presence of a pier (cf. Figure 1), which certainly exerts an influence in the development of the sliding surface.

In summary, the above numerical simulations provide justification for a plausible failure mechanism involving (i) the occurrence of progressive failure in the rock cliff, due to the gradual decrease of rock strength and deformability characteristics to critical values, and (ii) the subsequent development of a continuous sliding surface in the debris deposit, as observed in the field (Section 2).

a)

b)

Figure 11. Simulated a) displacements and b) plastic points
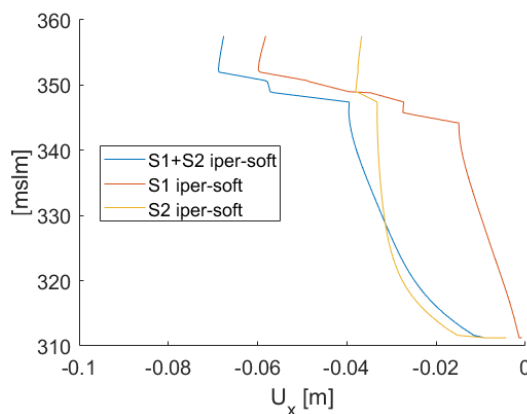

Figure 12. Numerically simulated accumulated displacements.

7

7 CONCLUSIONS

Field evidence gathered from the V70 landslide site shows the existence of a complex, slow deformation mechanism involving the presence of one or more sliding surfaces, as well as the interaction between a rock cliff and the underlying debris deposit.

In this work a preliminary numerical interpretation is provided for the complex landslide at hand, including an initial rock degradation phase and the subsequent development of rupture surfaces both in the rock and loose debris material. The presence of viaduct piers located at the toe of the slope was not included in the analysis at this stage. In such complex situation, a particularly challenging task was obtaining an initial stress state via geostatic calculations that was relatively free from plastic points. This was addressed by carrying out a parametric study on a simplified geometry characterised by two materials with large stiffness contrast. Then, the development of slope deformation over two geological phases in succession was simulated, showing that the occurrence of rupture surfaces in the rock cliff may bring about the onset of localised deformation within the underlying debris. Comparison between simulations and field evidence in terms of accumulated displacements over depth shows that the proposed numerical interpretation is plausible.

Future work will involve a more accurate numerical modelling of the different geological phases, as well as bespoke numerical analysis of the interaction between the debris slope and the viaduct piers located at its toe.

9 REFERENCES

Hoek, E., Carranza-Torres, C., and Corkum, B. (2002). Hoek-brown failure criterion. *Proceedings, NARMS-TAC Conference*, volume 1, 267-273, Toronto.

Lebourg, T., Mickael, H., Hervé, J., Samyr, E.B., Thomas, B., Swann, Z., Emmanuel, T. & Maurin V. 2011. Temporal evolution of weathered cataclastic material in gravitational faults of the La Clapiere deep-seated landslide by mechanical approach, *Landslides* **8**, 241–252.

Simeoni, L. & Ferro, E., 2015. Displacement rates of extremely slow landslides. *Proceedings, ECSMGE 2015*, Edinburgh (UK), 13-17 September 2015, 1879-1884.

Simeoni, L., Ronchetti, F., Corsini, A., Mongiovì, L., 2015. Partial reactivation of a DGSD of ignimbrite and tuff in an alpine glacial valley in Northern Italy. *Proceedings, Workshop on Volcanic Rocks and Soils*, Isle of Ischia, Italy, 24-25 September 2015 (Eds: Rotonda T., Cecconi M., Silvestri F. & Tommasi P.), 431-438.